# Biochar of Orange Peel as an Adsorbent for the Uptake of Lead (II) Ions

Ghaferah H. Al-Hazmi,[a] Lamia A. Albedair,[b] Edwin Andrew Ofudje ,[c] Moamen S. Refat,[d] Kholoud K. Alzahrani,[e] Ali El-Rayyes,[f] and Emmanuel Kola Oladejo [c]

Prepared orange peel biochar (OPB) was evaluated as a low-cost adsorbent for removing Pb(II) ions from aqueous solutions. The OPB was examined using scanning electron microscopy, Fourier transform infrared spectroscopy, thermal gravimetric analysis, and Brunauer-Emmett-Teller analysis to identify surface morphology, functional groups, thermal stability, and surface porosity responsible for adsorption, respectively. The biochar showed typical lignocellulosic decomposition behavior and exhibited a microporous surface whose hydroxyl, carbonyl, carboxylate, and phenolic groups allowed effective $Pb^{2+}$ uptake. Batch studies revealed maximum $Pb^{2+}$ at a pH 5, adsorbent dosage of 0.7 g, contact time of 80 min, adsorbate concentration of 150 mg/L, and temperature of 50 °C. The Langmuir isotherm revealed adsorption maximum capacity of the adsorbent to be 73.5 mg/g, while thermodynamics analysis showed that Pb(II) uptake was endothermic. These results demonstrate that orange-peel biochar can be an effective, environmentally friendly, and renewable adsorbent for lead ions in wastewater treatment.

*DOI: 10.15376/biores.21.2.3831-3855*

*Keywords: Adsorption; Isotherm; Kinetics; Lead (II) ions; Orange peel biochar; Wastewater*

*Contact information: a: Department of Chemistry, College of Science, Princess Nourah bint Abdulrahman University, P.O. Box 84428, Riyadh 11671, Saudi Arabia; b: Department of Chemistry, College of Science, Princess Nourah bint Abdulrahman University, P.O. Box 84428, Riyadh 11671, Saudi Arabia; c: Department of Chemical Sciences, Mountain Top University, Ibafo, Ogun State, Nigeria; d: Department of Chemistry, College of Science, Taif University, P.O. Box, 11099, Taif 21944, Saudi Arabia; e: Department of Biology, University College of Umluj, University of Tabuk, Umluj, Tabuk, Saudi Arabia; f: Center for Scientific Research and Entrepreneurship, Northern Border University, 73213, Arar, Saudi Arabia*;
** Corresponding author: kolaoladejo7@gmail.com*

## INTRODUCTION

Water is the most essential resource for human survival, but it is being polluted by waste from industrial, agricultural, and household activities, posing a serious risk to the aquatic ecosystem (John *et al*. 2019). Industrial activities, including fertilizer production, leather tanning, electroplating, textile manufacturing, sugar processing, metal processing, mining, and municipal waste management release harmful pollutants into water bodies (Raman *et al*. 2018; Akhtar *et al*. 2021). Among the contaminants released, toxic metals pose a severe threat to aquatic life, plants, humans, and animals' health. Their discharge into water systems through industrial actions is a pressing issue, causing irreversible damage to the ecosystems (Vidal *et al*. 2019; Briffa *et al*. 2020). Industrial wastewater often contains toxic heavy metal ions including lead, cadmium, arsenic, mercury, and chromium, which are harmful to aquatic life and are threatening to human health (Lupa *et*

*al*. 2018; Ghori *et al*. 2019; Balali-Mood *et al*. 2021). Food crops grown on metal-contaminated soil can become toxic, posing serious health risks to humans who consume them, which can lead to nutritional deficiencies and a range of health problems (Khan *et al*. 2019).

Among these pollutants, lead is particularly of great concern because of its widespread industrial use in batteries, paints, alloys, and electroplating processes (Colin *et al*. 2022). Lead residues released into water bodies can accumulate in aquatic ecosystems, ultimately entering the human food chain and posing great health risks (Mishra *et al*. 2019). Even at trace levels, lead exposure can lead to severe health effects, such as hypertension, nephritis, constipation, stomach pain, nausea, vomiting, neurological issues, speaking difficulties, renal, and reproductive disorders (Chowdhury *et al*. 2022; Rahman *et al*. 2023; Zheng *et al*. 2024). Therefore, the discharge of lead-containing effluents into water bodies poses a severe risk to both ecosystems necessitating the development of efficient and sustainable removal strategies to ensure safe drinking water and human health protection (Chowdhury *et al*. 2022).

Conventional treatment methods for lead removal from wastewater include chemical precipitation (Zheng *et al*. 2024), ion exchange (Jasim and Ajjam 2024), coagulation-flocculation (Benalia *et al*. 2024), membrane filtration (Azmi 2025), and others. However, they often suffer from high operational costs, incomplete pollutant removal, and secondary pollution generation (Arogundade *et al*. 2025). The adsorption technique has emerged as a highly effective technique for removing lead ions and other contaminants from wastewater, garnering attention due to its effectiveness and potential for efficient and sustainable remediation (Jjagwe *et al*. 2021). Despite the numerous advantages offered by adsorption techniques, its high cost of production often limits the full application most especially in developing countries such as Nigeria.

Recently, carbon-rich material, also known as biochar, that is often obtained from biomass pyrolysis, has appeared as a promising low-cost adsorbent to remove pollutants from wastewater because of its porous structure, abundance of functional groups, and high surface area, which enhance its adsorption capacity (Meng *et al*. 2025). Various by-products of agricultural origin, such as rice husk (Gargiulo *et al*. 2024), coconut shell (Minh *et al*. 2023), corn cob (Onyekwere *et al*. 2024), banana peel (Negroiu *et al*. 2021), and *Manihot esculenta* (El-Rayyes *et al*. 2025), have been successfully examined for the elimination of heavy metals. These eco-friendly adsorbents are abundant and more cost-effective than traditional activated carbon. Their application puts the concept of waste valorization and circular economy into practice (Wang *et al*. 2022).

Another readily available lignocellulosic agricultural waste with high carbon content that is yet to be explored fully is orange peel. Orange peel is a common agro-waste generated in large quantities by fruit processing industries, and it is mostly disposed of in landfills or burned in open air, which poses serious environmental pollution, such as the generation of greenhouse gases (Afolabi and Musonge 2023). However, it represents a valuable and underutilized source of biomass for biochar production (Michael-Igolima *et al*. 2023). It contains high amounts of cellulose, hemicellulose, lignin, and functionalized organic compounds that can enhance metal binding when carbonized (Zhang *et al.* 2022; Mousa *et al*. 2025). Converting orange peel into biochar not only provides a sustainable waste management strategy but also supports the principles of circular economy by transforming waste into a resource for environmental remediation. Biochars of orange-peel-derived origins have been widely studied for heavy metal removal because of their abundance of oxygen-containing functional groups and lignocellulosic composition. But,

many of these findings have focused primarily on achieving high removal efficiencies without establishing internal consistency between experimental adsorption capacity, kinetic transport regimes, isotherm-derived parameters, and thermodynamic behavior. In some cases, the production of the biochar is done at elevated temperature.

The current study investigates the potential of biochar derived from orange peel as an active material for lead ion uptake from aqueous solutions. The study evaluates the impact of process parameters of solution pH, adsorbent dosage, temperature, contact time, and concentration as they relate to the adsorption of the adsorbate. The adsorption process mechanisms were also examined using various adsorption kinetics, isotherms, and thermodynamic investigations.

## EXPERIMENTAL

### Materials

Fresh orange peels were collected from a fruit store in Ibafo, Ogun State, Nigeria. Thereafter, distilled water was used to thoroughly wash the sample to eliminate dirt and other impurities. After washing, the materials was air-dried for 7 days.

Stock solution of $Pb^{2+}$ ions were prepared using analytical grade lead (II) nitrate [$Pb(NO_3)_2$] procured from Merck, Germany. Hydrochloric acid (HCl: 37%) and sodium hydroxide (NaOH: 98%) were purchased from Sigma-Aldrich, India, and used for pH adjustment.

### Preparation Of Orange Peel Biochar

The cleaned and oven-dried orange peels (105 °C for 24 h) were then reduced to powder using a mortar and pestle. The powdered orange peel was converted into biochar through pyrolysis in a muffle furnace under limited oxygen at 500 °C for 2 h. The biochar was repeatedly washed with distilled water to eliminate residual ash and soluble impurities, then oven-dried again (105 °C) and stored in airtight containers for further use.

### Characterization of the Biochar

Fourier transform infrared (FT-IR) analysis was performed to detect the metal ion binding functional groups available on the surface of the biochar. The FT-IR analysis was conducted using an FT-IR spectrometer (PerkinElmer Spectrum 2, USA) within the range of 4000 to 400 $cm^{-1}$. Finely ground samples were mixed with KBr powder and compressed into pellets before analysis.

To observe the surface morphology of the biochar by scanning electron microscopy (SEM), the samples were first coated with a thin layer of gold to improve conductivity. The SEM device was a JEOL JSM-5600 (Tokyo, Japan). The Brunauer–Emmett–Teller (BET) technique was employed for determined the pore size distribution and surface area using a Quantachrome NOVA 2200C instrument (USA).

Thermogravimetric investigation (TGA 4000, PerkinElmer, Haarlem, Netherlands) was performed under a nitrogen atmosphere from room temperature to 800 °C at a heating rate of 10 °C/min to evaluate the thermal stability characteristics of the orange peel.

The point of zero charge (pHpZc) of the OPB was measured using the pH-drift technique. A total of 25 mL of NaCl solutions (0.01 M) were adjusted in the pH range of 2 to 8, and thereafter, 5 mg of biochar was added and shaken for 12 h at 150 rpm.

Thereafter, the pH was recorded again and the changes between the first and the last pH; ($\Delta pH = pH_f - pH_o$) were plotted against $pH_o$ to determine the pHpZc.

## Preparations of Lead Solutions

A total of 1.60 g of $Pb(NO_3)_2$ was dissolved in 1000 mL of distilled water for the preparation of 1000 mg/L stock solution of $Pb^{2+}$. Different working solutions in the range of 10 to 150 mg/L were prepared *via* serial dilution of the stock solution. The adjustment of pH of the solution was made using 0.1 M HCl or NaOH.

## Batch Adsorption Studies

Batch sorption studies were conducted in triplicate, and the average values were recorded to estimate the efficiency of OPB for $Pb^{2+}$ removal. In each run, 0.7 g of OPB was contacted with 50 mL of $Pb^{2+}$ solution (150 mg/L) in a conical flask, and the solution pH was adjusted as desired. Thereafter, agitation of the mixture on a rotatory orbital shaker at a constant speed of 100 rpm was done for a predetermined contact time within the range of 10 to 120 min at room temperature. After the attainment of equilibrium, the content was filtered, and the residual lead content in the filtrate was determined using an Atomic Absorption Spectrophotometer (AAS) (Jenway 7325, UK). The percentage removal (%) and adsorption capacity ($q_e$, mg/g) were determined by adopting Eqs. 1 and 2, respectively,

$$R(\%) = \frac{C_o - C_e}{C_o} \times 100 \quad (1)$$

$$q_e = \frac{C_o - C_e}{m} \times v \quad (2)$$

where $C_0$ and $C_e$ are $Pb^{2+}$ concentrations at initial and equilibrium stages in mg/L, and $V$ and $m$ are the volume of the solution (L) and OPB mass (g), respectively.

## Adsorption Modeling

*Adsorption kinetics*

The sorption kinetics were characterized using linearized forms of pseudo-first-order, pseudo-second-order, and intraparticle diffusion kinetics models (Eqs. 3 to 5) (Chen *et al*. 2019; Mustapha *et al*. 2021; El Hammari *et al.* 2022; Ademoyegun *et al*. 2022; Ofudje *et al*. 2024). These models are used to describe the rate of $Pb^{2+}$ ions adsorption onto the OPB surface.

$$\ln(q_e - q_t) = \ln q_e - k_1 t \quad (3)$$

$$\frac{t}{q_t} = \frac{1}{k_2 q_e^2} + \frac{t}{q_e} \quad (4)$$

$$q_t = k_p t^{1/2} + C_i \quad (5)$$

In the above equations, $q_e$ and $q_t$ represent the quantities of $Pb^{2+}$ adsorbed at equilibrium (mg/g) and at time $t$ (min), respectively. The $k_1$ and $k_2$ represent the pseudo-first and pseudo-second order adsorption rate constants in $min^{-1}$ and (g/mg min) respectively, $k_p$ stands for rate constant of intra-particle diffusion ($mg/g/min^{1/2}$), and $C_i$ represents the boundary layer thickness effect (intercept). The best model fit is determined by the highest correlation coefficient ($R^2$) and lowest Sum of squared error (SSE) value, indicating the

most accurate description of adsorption kinetics under the studied conditions. The SSE values for adsorption capacity were calculated using Eq. 6 (Ofudje *et al*. 2023),

$$SSE = \sum_{i=1}^{N} (q_{e(exp.)} - q_{e(cal.)})^2 \quad (6)$$

where N represents the number of data points.

## Adsorption Isotherm

The Langmuir isotherm (Eq. 7) assumes monolayer adsorption on homogeneous adsorbent sites, and is given as (Mustapha *et al*. 2021; Ademoyegun *et al*. 2022):

$$C_e/q_e = C_e/Q_{max} + 1/Q_{max}K_L \quad (7)$$

The dimensionless separation factor $R_L$ from the Langmuir isotherm model indicates adsorption favorability and was estimated using Eq. 8 below (Din *et al*. 2025),

$$R_L = 1/(1+bC_0) \quad (8)$$

where $q_e$, $C_e$ and $C_0$ are as previously defined, $Q_{max}$ defines the maximum adsorption capacity (mg/g), and $K_L$ is the Langmuir adsorption constant (L/mg).

The Freundlich isotherm model (Eq. 9) describes sorption on heterogeneous surfaces (Aderibigbe *et al*. 2024; Ofudje *et al.* 2024),

$$lnq_e = lnK_F + \frac{1}{n} lnC_e \quad (9)$$

where the Freundlich constant is given as $K_F$ (mg/g), which is related to the adsorption capacity, and the dimensionless constant that reflects the adsorption intensity is given as $n$. Insight into the nature of the sorption process is provided by the value of $n$, where $n = 1$ implies linear adsorption, $n < 1$ suggests favorable adsorption, and $n > 1$ suggests weak adsorption.

The Dubinin-Radushkevich (D-R) isotherm (Eq. 10) assesses adsorbate-adsorbent interactions, estimates adsorption free energy, and distinguishes between chemical and physical adsorption mechanisms based on the Polanyi potential theory. It is useful for analyzing adsorption across concentrations and understanding adsorbent porosity (Ghosh *et al*. 2023). Equation 10 is given as,

$$lnq_e = lnq_o - K\epsilon^2 \quad (10)$$

where $q_e$ is as previously defined, $q_o$ denotes maximum adsorption capacity (theoretical) (mg/g), and $K$ is the D-R constant that reflects the adsorption energy (mol²/J²).

The mean adsorption energy, $E$, indicates the adsorption process type, and it is calculated as:

$$E = \frac{1}{\sqrt{2K}} \quad (11)$$

The $E$ values classify the mechanism, where 0 to 8 kJ/mol implies physisorption, and $E >$ 16 kJ/mol implies chemisorption, according to Ofudje *et al.* (2023).

*Adsorption thermodynamics*

The parameters from thermodynamic analysis, which include enthalpy ($\Delta H$), Gibbs free energy ($\Delta G$), and entropy ($\Delta S$), were determined using Eqs. 12 and 13 (Bouguettoucha *et al.* 2015; Ogundiran *et al*. 2022; Kori *et al*. 2024; Din *et al*. 2025),

$$\Delta G^o = -RT\ln K_D \quad (12)$$

$$\ln(\rho K_D) = -\frac{\Delta H}{RT} + \frac{\Delta S}{R} \quad (13)$$

where $T$ is the absolute temperature (K), $\rho$ is the water density (g/L), $R$ is the universal gas constant, and $K_D$ denotes the equilibrium constant.

## Reusability and Regeneration Studies

The reusability and regeneration of orange peel biochar were examined to assess its potential for repeated applications in lead ion removal. Following each adsorption cycle, the biochar was desorbed using a 0.1 M acetic acid solution, subsequently cleansed using distilled water, and then dried for 12 h in an oven at 105 °C. The regenerated biochar was used in the subsequent experiments under constant parameters, such as a biochar dosage of 1 g, $Pb^{2+}$ concentration of 150 mg/L, a pH of 5, a contact time of 80 min, and a temperature of 50 °C. This procedure was conducted for five consecutive cycles, and the recovery efficiency (%RE) was estimated from Eq. 14:

$$\%\,RE = \frac{amount\ desorbed}{amount\ adsorbed} \times 100 \quad (14)$$

## Effect of Competing Ions

To assess the applicability of OPB under realistic water condition, competitive adsorption experiments were performed in the presence of representative background electrolytes and co-contaminants commonly found in natural and wastewater systems. Batch adsorption tests were done at the optimized conditions (pH 5, $Pb^{2+}$ = 150 mg/L, OPB dosage = 0.7 g, contact time = 80 min, 50 °C), with the addition of $Mg^{2+}$ and $Ca^{2+}$ (50 mg/L each), carbonate ($CO_3^{2-}$), sulfate ($SO_4^{2-}$), chloride ($Cl^-$), and natural organic matter (NOM, 10 mg/L as humic acid).

# RESULTS AND DISCUSSION

## The Role of $Pb^{2+}$ Initial Concentration and Agitation Time

The impact of agitation time (10 to 120 min) as well $Pb^{2+}$ initial concentration (10 to 150 mg/L) was studied, while keeping other parameters constant (Fig. 1). It was noted that during the first 30 min, the amount adsorbed increased rapidly because of the large amount of unfilled binding sites on OPB's surface that easily attract $Pb^{2+}$ molecules (Ofudje *et al*. 2024).

Nonetheless, as the reaction continues, the sites become occupied, and the adsorption rate slows down, gradually reaching equilibrium (Ofudje *et al*. 2024). This is evidenced with a maximum adsorption of 69.6 mg/g at $Pb^{2+}$ concentration of 150 mg/L and 80 min.

At lower concentrations, adsorption capacities were reduced compared to higher concentrations, indicating that higher concentrations increase the driving force for mass

transfer, enabling more $Pb^{2+}$ ions to react with available adsorption sites of the biochar surface (Mandal *et al*. 2021).

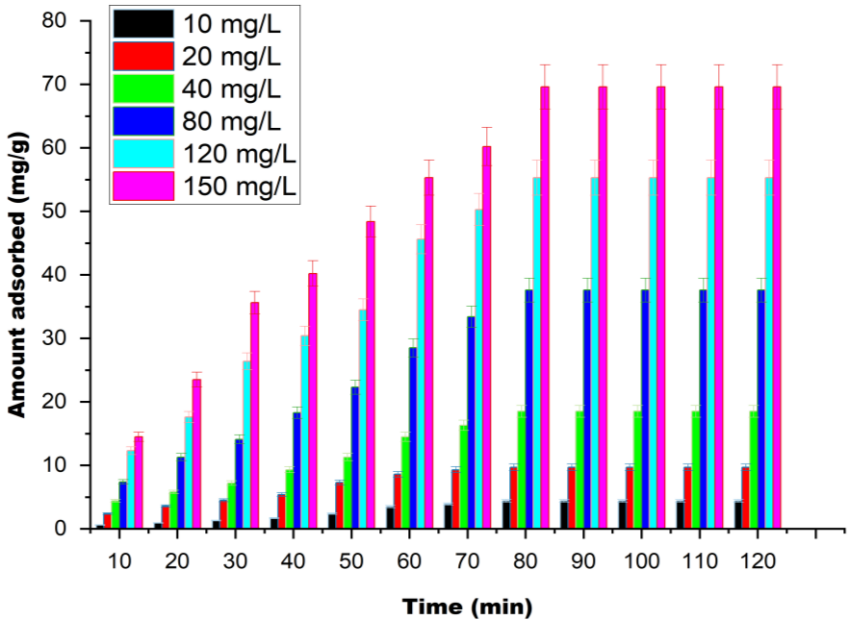


**Fig. 1.** Influence of $Pb^{2+}$concentration and agitation time on the sorption capacity of OPB

## Impact of Solution pH

The solution pH influences both the adsorbent's surface charge and the ionization degree of the adsorbate in the adsorption of lead ions. Figure 2 shows the percentage removal variation of $Pb^{2+}$ by OPB across different pH values ranging from 2 to 8, while other variables were kept constant.

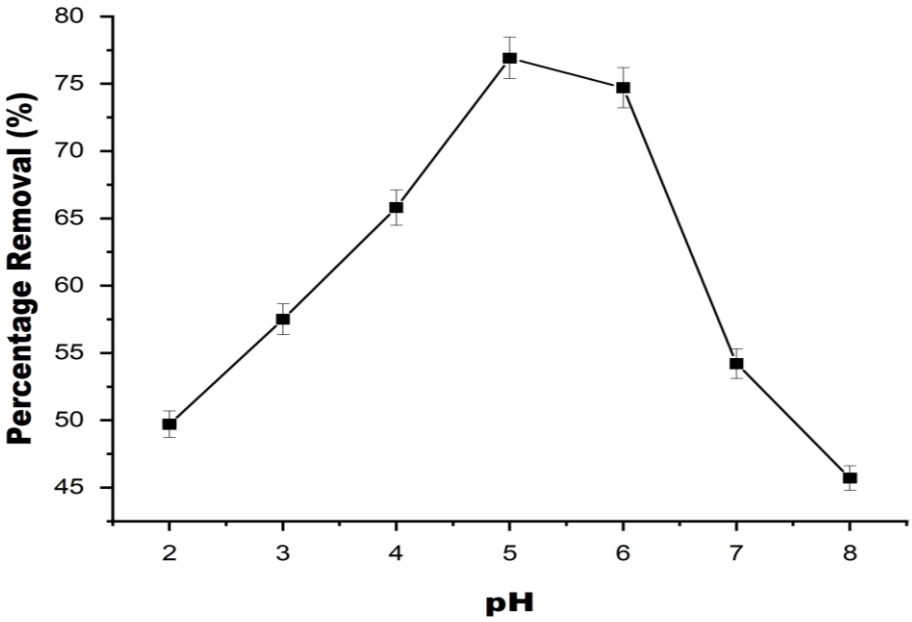


**Fig. 2.** Influence of solution pH on the adsorption of $Pb^{2+}$ onto OPB

It was noted that the adsorption efficiency rose steadily from 49.6% at pH 2 to 77.8% at pH 5, after which it declined to 45.2% at pH 8. This behavior can be because of the electrostatic interactions between the surface of the adsorbent and the molecules of the metal ion (Ngueagni *et al*. 2025). This behavior is consistent with the value of the zero-point charge measured (pHpZc = 3.5), suggesting the OPB surface to be positively charged at a pH lower than 3.5 and negatively charged when above it. At lower pH, the OPB's surface is highly protonated because of high $H^+$ ions concentration, resulting in an electrostatic repulsion of the $Pb^{2+}$ on the surface of the biochar (Ngueagni *et al*. 2025). However, with a rise in the pH, the surface charge gradually becomes less positive, enhancing electrostatic attraction and $Pb^{2+}$ uptake.

Optimum adsorption efficiency was observed at pH 5, with a percentage removal of 77.8 %. Above pH 5, the adsorption efficiency decreases because of the increase in the formation of $Pb(OH)_2$, which reduces the adsorbent's affinity for the positively charged metal ions (Singh *et al*. 2023). Ngueagni *et al*. (2025) also reported the same observation, confirming the pH-dependent nature of the adsorption process.

## Influence of Temperature

The effect of temperature on the sorption of $Pb^{2+}$ by the OPB was investigated over the 25 to 65 °C range while other variables were kept constant as presented in Fig. 3. As seen in the plot, the percentage removal increased from 54 % at 25 °C to a maximum of 82% at 55 °C. At the initial level, increasing temperature enhances the mobility of $Pb^{2+}$ ions and improves their diffusion into the internal pores of the biochar.

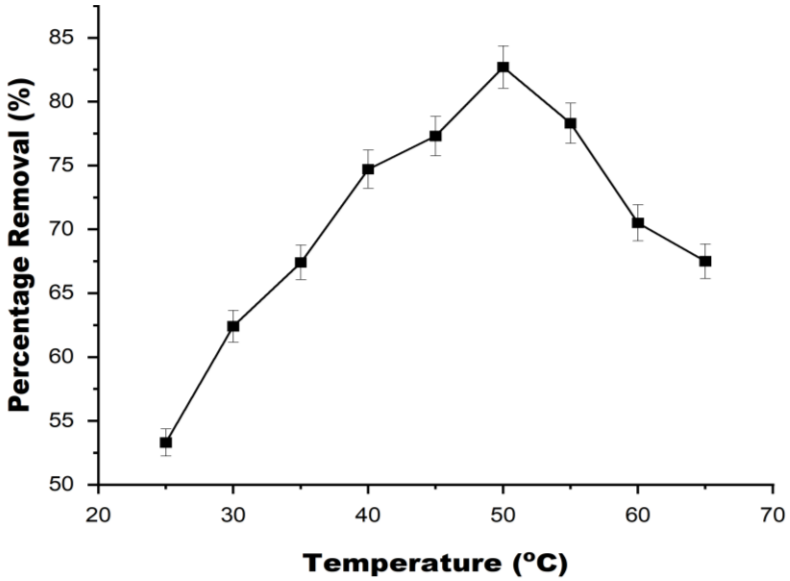


**Fig. 3.** Influence of temperature on the sorption of $Pb^{2+}$ by OPB

## Adsorption Kinetics

The linearized plots for the sorption kinetics of $Pb^{2+}$ onto OPB are shown in Figs. 4 to 6, and the parameter values are provided in Table 1. The three models applied suitably explain the adsorption process, as evidence from the high values of coefficient of determination ($R^2$).

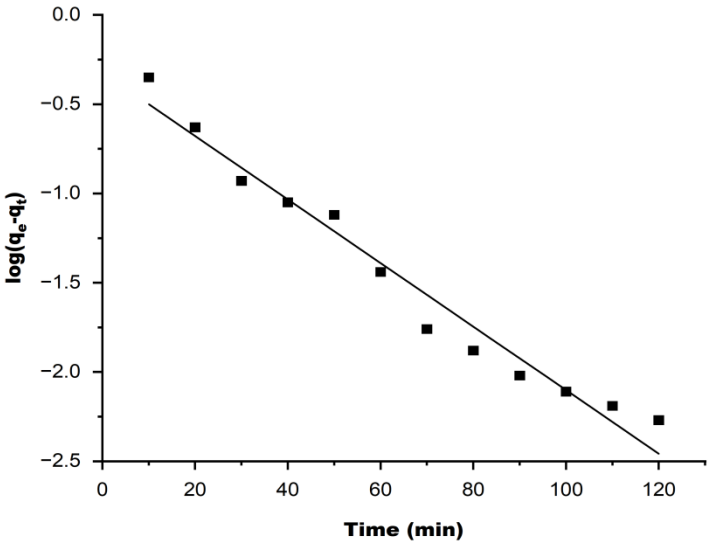


**Fig. 4.** Pseudo-first-order kinetic plot for $Pb^{2+}$ sorption by OPB

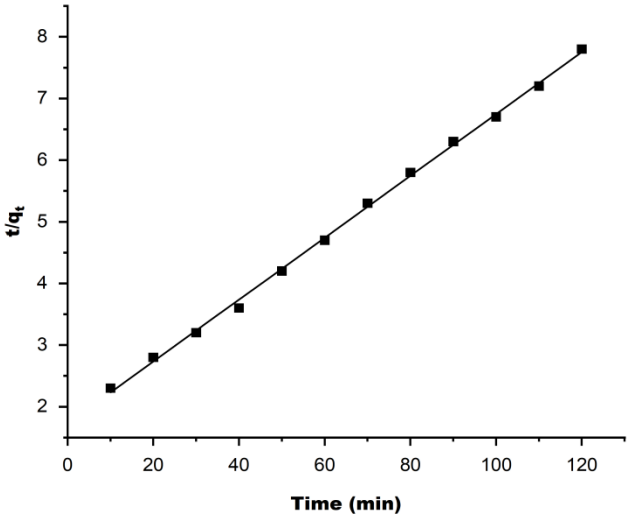


**Fig. 5.** Pseudo-second-order kinetic plot for $Pb^{2+}$ sorption by OPB

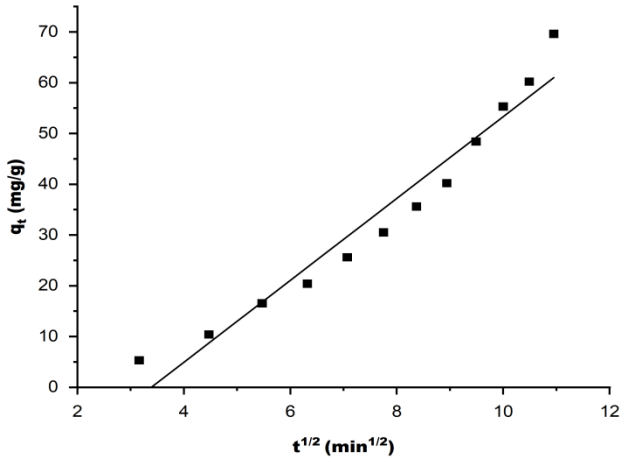


**Fig. 6.** Intraparticle diffusion plot for $Pb^{2+}$ sorption by OPB

**Table 1.** Kinetics Parameters for $Pb^{2+}$ Sorption by OPB

| | | First-order | | | | Second-order | | | | Intra Particle Diffusion | | |
|---|---|---|---|---|---|---|---|---|---|---|---|---|
| $C_e$ (mg/L) | $Q_e$(exp) (mg/g) | $Q_e$(cal) (mg/g) | $k_1$ ($min^{-1}$) | $R^2$ | SSE | $Q_e$(cal) (mg/g) | $k_2$ (g/mg min) | $R^2$ | SSE | $K_p$ ($mg/g/mins^{1/2}$) | $C_i$ (mg/g) | $R^2$ |
| 7.2 | 4.400 | 7.300 | 0.309 | 0.937 | 0.099 | 4.2 | 0.503 | 0.965 | 0.014 | 2.682 | 0.307 | 0.955 |
| 15.3 | 9.700 | 13.300 | 0.437 | 0.966 | 0.052 | 8.9 | 0.581 | 0.996 | 0.025 | 4.06 | 0.395 | 0.945 |
| 24.5 | 18.500 | 22.100 | 0.611 | 0.928 | 0.059 | 18.1 | 0.612 | 0.988 | 0.017 | 7.806 | 1.412 | 0.965 |
| 44.5 | 37.600 | 32.500 | 0.662 | 0.935 | 0.041 | 36.9 | 0.684 | 0.996 | 0.026 | 8.658 | 1.611 | 0.975 |
| 53.5 | 55.300 | 49.300 | 0.708 | 0.956 | 0.033 | 54.2 | 0.722 | 0.979 | 0.016 | 8.851 | 2.051 | 0.976 |
| 70.3 | 69.600 | 59.400 | 0.759 | 0.913 | 0.044 | 70.1 | 0.859 | 0.996 | 0.002 | 12.024 | 2.492 | 0.946 |

The pseudo-second-order showed the highest value. In addition, the near agreement between the experimental adsorption capacity ($Q_{e,\ exp.}$) and the calculated equilibrium capacities ($Q_{e,\ cal.}$) further support the suitability of the pseudo-second-order model. The value of $R^2$ obtained affirmed that intraparticle diffusion also contributes to the sorption process, but it is not the only rate-limiting step, as plots do not pass through the origin (Fig. 6). This deviation implies that external mass transfer, boundary layer diffusion, and interactions taking place on the surface, such as hydrogen bonding and ion exchange, also play key roles (Arogundade *et al*. 2025). Both the pseudo–first-order and pseudo–second-order kinetic models, as well as the intra-particle diffusion model, showed a good fit for lead ion adsorption onto the biochar, with high $R^2$ values ($R^2 > 0.9$). This combination of findings implies that the sorption rate is mainly controlled by diffusion processes and that interactions between the molecules of the adsorbate occur within the material's porous structure (Hubbe *et al*. 2019). The cited work also showed that a mistake had been made during the original derivation of the pseudo-second order model. The fact that the expression happens to fit many data sets for adsorption onto porous materials appears to have been a matter of luck.

## Adsorption Isotherms

The equilibrium data for the adsorption of $Pb^{2+}$ onto orange peel biochar (OPB) were evaluated using three prominent isotherm models as depicted graphically in Figs. 7 to 9, with their corresponding parameters presented in Table 2.

The Langmuir isotherm gave a reasonable fit to the experimental data, yielding a maximum adsorption capacity ($Q_{max}$) of 73.5 mg/g with $R^2$ value of 0.956. With this, the Langmuir model is seen as an effective saturation model, assuming a finite number of adsorption sites under fixed solution pH and temperature. The value of the separation factor ($R_L$) calculated using the highest initial $Pb^{2+}$ concentration ($C_0$ = 150 mg/L) was found to be 0.059, confirming that $Pb^{2+}$ adsorption on the biochar is favourable. The Freundlich model exhibited an excellent fit to the equilibrium data. Among the isotherm models, the Freundlich model demonstrated the best fit for the adsorption data, as indicated by its high coefficient of determination ($R^2$). This suggests that $Pb^{2+}$ adsorption occurs on a heterogeneous surface that contains multiple types of binding sites with varying affinities. The value of the Freundlich dimensionless parameters ($1/n$), which is less than 1, indicates a strong adsorption intensity, suggesting that the sorption is favourable.

The D–R isotherm model gave insight into the nature of the sorption mechanism. The mean free energy of adsorption ($E$) was calculated to be 0.495 kJ/mol, which is well below the threshold of 8 kJ/mol for physisorption (Mohrazi and Ghasemi-Fasaei 2023; Arogundade *et al*. 2025). This low value indicates that the uptake of $Pb^{2+}$ onto OPB also proceeds through physical adsorption mechanisms (Dubinin 1960; Mohrazi and Ghasemi-Fasaei 2023). Therefore, the equilibrium behavior is accredited to weak van der Waals forces, electrostatic attraction, and pore-filling effects rather than specific chemical bonding. The comparison of the adsorption capacities from different adsorbents for the removal of $Pb^{2+}$ from wastewater is presented in Table 3. This comparison reinforces the suitability of OPB as a competitive and effective adsorbent for lead-contaminated wastewater.

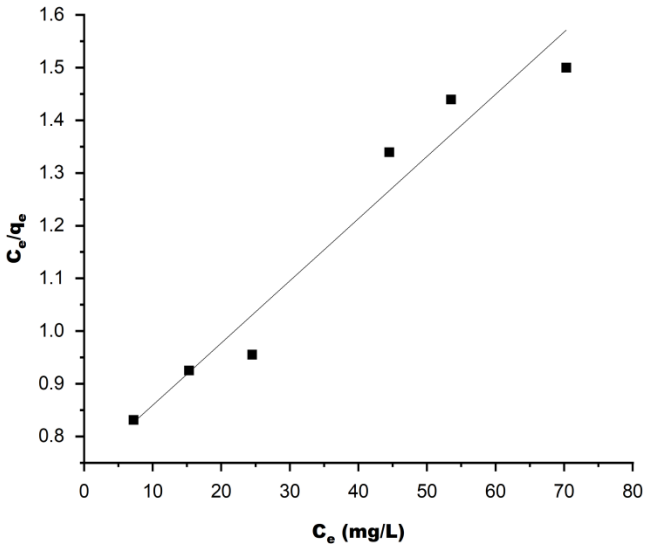


**Fig. 7.** Langmuir isotherm for the sorption of $Pb^{2+}$ onto OPB

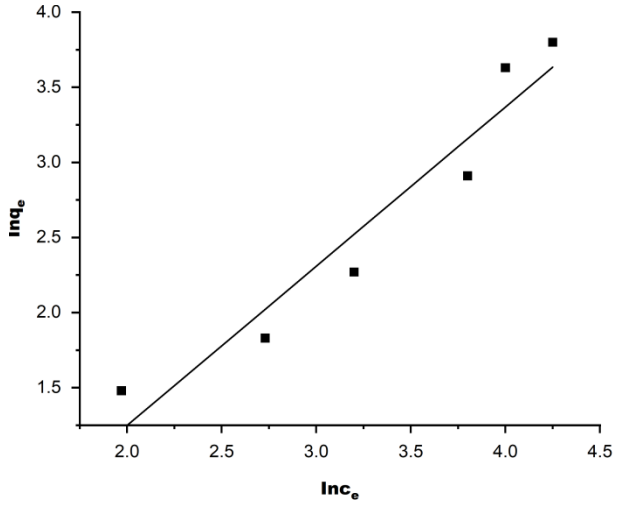


**Fig. 8.** Freundlich isotherm for the sorption of $Pb^{2+}$ onto OPB

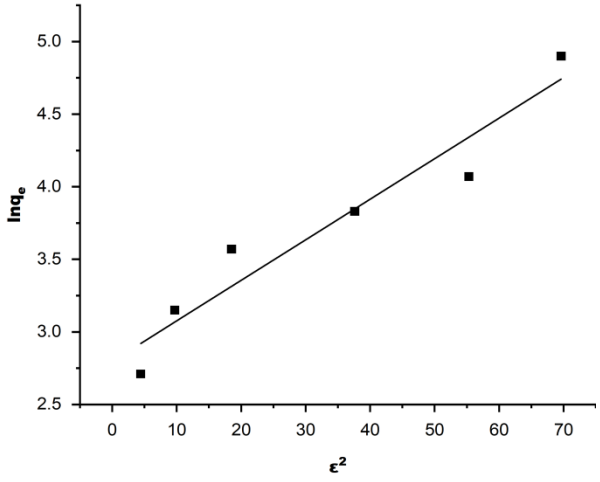


**Fig. 9.** Dubinin–Radushkevich isotherm for the sorption of $Pb^{2+}$ onto OPB

**Table 2.** Parameters from the Isotherm Analysis of the Sorption of $Pb^{2+}$ onto OPB

| Models | Parameters | OPB |
|---|---|---|
| Langmuir | $Q_{max}$ (mg/g) | 73.5 |
| | $R_L$ | 0.059 |
| | $R^2$ | 0.956 |
| Freundlich | $K_f$ ((mg/g)(mg/L)$^{-1/2)}$ | 40.24 |
| | 1/*n* | 0.105 |
| | $R^2$ | 0.996 |
| Dubinin–Radushkevich (D–R) | $Q_s$ | 56.503 |
| | *E* | 0.495 |
| | $R^2$ | 0.978 |

**Table 3.** Comparison of Various Adsorbents' Adsorption Capacities for $Pb^{2+}$ Uptake by OPB

| Adsorbent | Adsorption Capacity | References |
|---|---|---|
| *Manihot esculenta* chaff | 78.0 | El-Rayyes *et al*. 2025 |
| Carbonized sawdust | 87.7 | Aigbe and Kavaz (2021) |
| Banana peel | 39.3 | Afolabi *et al*. 2021 |
| Date seed biochar | 74.6 | Mahdi *et al*. 2018 |
| Calcium-phosphate hydroxyl | 15.1 | Arogundade *et al*. 2025 |
| *Quercus robur* | 63.6 | Mohubedu *et al*. 2019 |
| Pomelo peel | 88.7 | Zhao *et al*. 2018 |
| Pine sawdust | 99.5 | Niu *et al*. 2020 |
| Orange peel biochar (OPB) | 73.5 | This study |

## Thermodynamics Studies

Figure 10 illustrates the plot of the adsorption thermodynamics, while the parameters are presented in Table 4. The Gibbs free energy ($\Delta G°$) with negative value indicates that $Pb^{2+}$ adsorption on OPB was found to be a spontaneous process under all investigated temperatures.

The value of $\Delta G°$ gave an insight into the adsorption nature, with values ranging from −20 to 0 kJ/mol reflecting physisorption, while values in the range of −80 and −400 kJ/mol are indicative of chemisorption (Sireesha *et al*. 2025). Given that the range of $\Delta G°$ from this study falls in the range of physisorption, it can be inferred that the sorption of $Pb^{2+}$ is also governed by physical sorption process. The positive enthalpy change ($\Delta H°$) value confirms that the adsorption process is endothermic, which implies that energy input is required for effective adsorption (Ogundiran *et al*. 2022). The positive entropy ($\Delta S°$) value infers that during adsorption, there is an increase in randomness at the solid-liquid interface, which indicates greater disorder in the system as $Pb^{2+}$ is adsorbed onto the surface of the biochar.

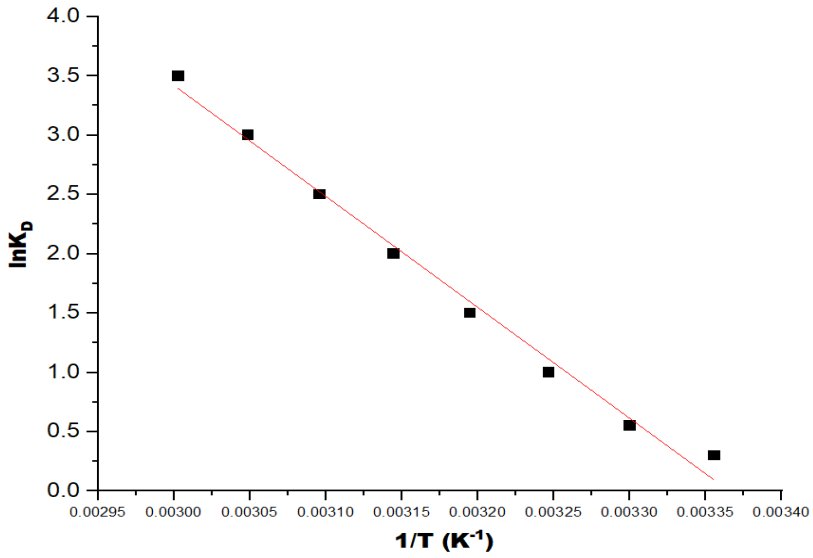


**Fig. 10.** Thermodynamic plot for the uptake of $Pb^{2+}$ onto OPB

**Table 4.** Parameters of Thermodynamic Analysis for the Sorption of $Pb^{2+}$ by OPB

| *T* (°C) | Δ*G*° (kJ/mol) | Δ*H*° (kJ/mol) | Δ*S*° (J/mol·K) |
|---|---|---|---|
| 25 | -0.25 | | |
| 30 | -0.44 | | |
| 35 | -0.84 | | |
| 40 | -1.05 | 14.25 | 0.049 |
| 45 | -1.35 | | |
| 50 | -1.74 | | |
| 55 | -2.02 | | |
| 60 | -2.33 | | |
| 65 | -2.84 | | |

## Regeneration and Reusability Studies

The desorption behaviour of $Pb^{2+}$ from OPB was evaluated over five consecutive adsorption–desorption cycles as shown in Fig. 11. It was observed that the recovery efficiency was 75.2% in the first cycle and gradually decreased to 65.1% by the fifth cycle. The steady decline observed across the cycles may arise from partial blocking of some active sites on the adsorbent surface during each adsorption cycle (Ofudje *et al*. 2023). The ability of the adsorbent to maintain efficiencies above 65% after five cycles indicates that OPB possesses a good level of stability and reusability. This supports its potential application as a low-cost and regenerable adsorbent for $Pb^{2+}$ removal in wastewater treatment systems.

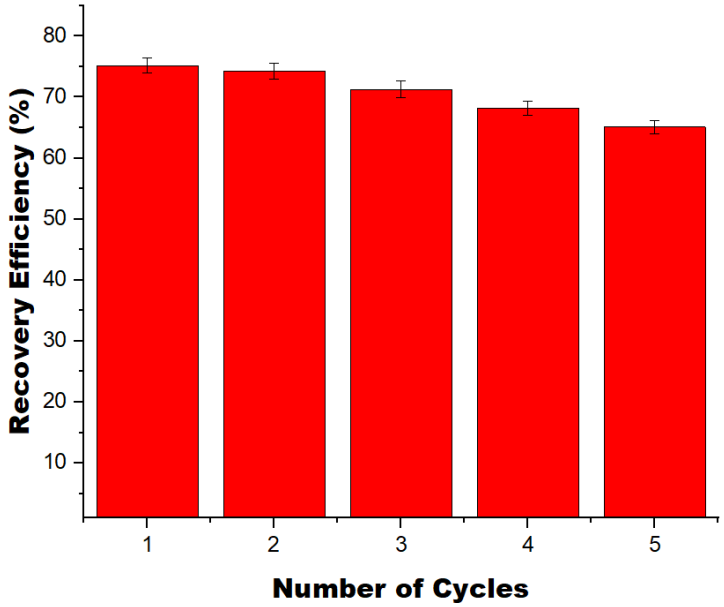


**Fig. 11.** Thermodynamic plot for the adsorption of $Pb^{2+}$ onto OPB

## Adsorption Mechanism

The combined kinetic modelling, isotherm analysis, and thermodynamic results suggest that the uptake of $Pb^{2+}$ onto the OPB proceeds through a multistep mechanism involving both physical and chemical interactions (Fig. 12).

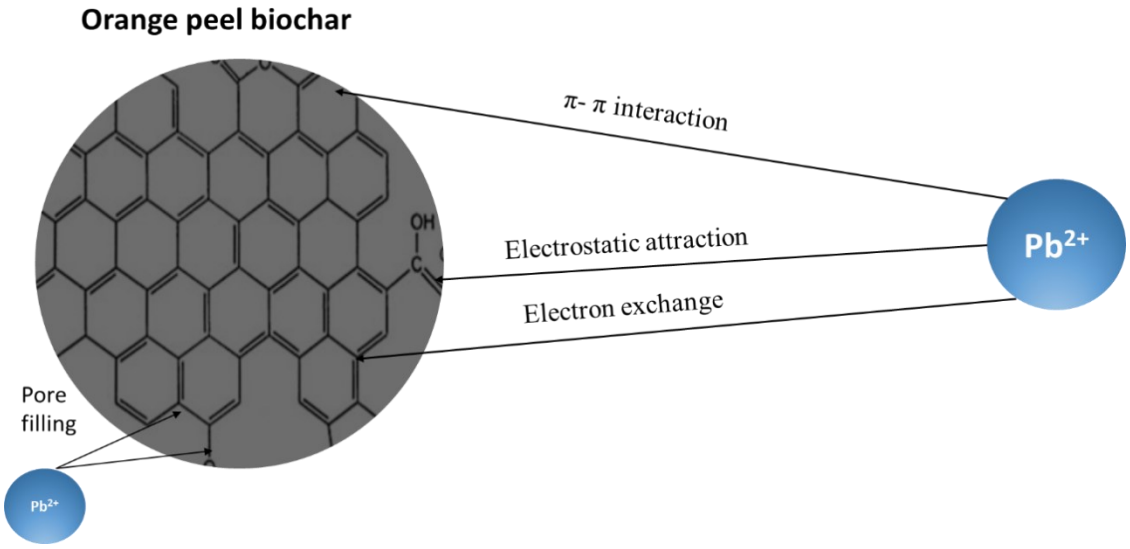


**Fig. 12.** Schematic representation of the adsorption mechanism of $Pb^{2+}$ onto OPB

These interactions allow $Pb^{2+}$ ions to interact with the functional groups on the OPB surface. The contribution of physical uptake is reflected in the Dubinin–Radushkevich (D–R) isotherm, where the mean free adsorption energy ($E$ = 0.495 kJ/mol) indicates that a portion of the process involves physisorption through weak electrostatic attractions. The equilibrium modelling revealed that both the Langmuir and the Freundlich models fit the

data well. This combination supports a dual mechanism where $Pb^{2+}$ ions first attach to high-affinity sites through complexation, followed by additional uptake into pores and lower-affinity regions through physical interactions. Thermodynamic results from free energy and enthalpy changes also corroborated the fact that the process is controlled by physisorption.

## BET Analysis

The BET analysis gave the pore-size distribution, as revealed in Fig. 13. It showed that the orange peel biochar structure is dominated by micropores (< 2 nm), with a transition toward small mesopores as the pore diameter increased in biochars derived from lignocellulosic material. Such a distribution contributed meaningfully to a high specific surface area (72.1 $m^2/g$), which favored the adsorption of contaminants. This aligns with a literature report on orange-peel biochar systems, where KOH activation effectively improves pore volume and microporosity (Zhang *et al.* 2022). The high density of narrow pores around 0.25 to 0.35 nm is likely attributed to the rearrangement of carbon domains during thermal activation, similar to those properties reported for citrus-based biochars by Nandiyanto *et al.* (2025).

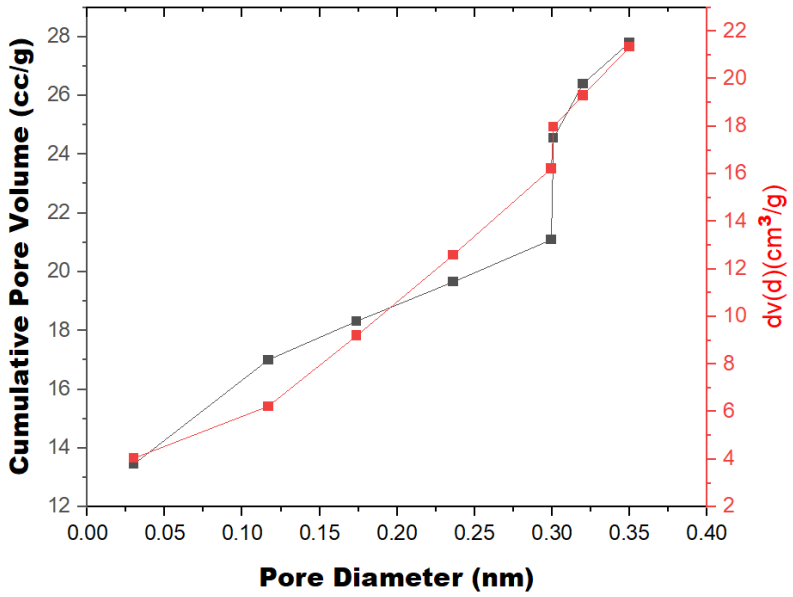


**Fig. 13.** The pore size distribution analysis of orange peel biochar

## Discussion on TGA

The thermogravimetric analysis (TGA) curve of orange peel showing multistage thermal degradation pattern characteristic is depicted in Fig. 14. An early small weight loss was seen below 120 °C, which is attributed to the evaporation of physically adsorbed moisture (Kordoghli *et al*. 2023; Mousa *et al*. 2025). This accounted for 5 to 10% mass loss and is consistent with the lignocellulosic biomass nature of citrus residues. A steady weight loss from 120 °C to around 250 °C reflects the decomposition of hemicellulose, which begins at lower a temperature because of its amorphous and thermally unstable nature. A huge weight-loss was seen around 250 and 350 °C, indicating hemicellulose and cellulose degradation (Kordoghli *et al*. 2023; Mousa *et al*. 2025). This sharp decline is

characteristic of citrus peels, where cellulose depolymerization and the breakdown of pectin-rich cell walls lead to the release of some volatiles. The maximum rate of devolatilization is evidence from the sharpest inflection point in this region. Above 350 °C, the curve displayed a slower, and gradual mass loss up to 450 °C, which was indicative of the decomposition of lignin components (Kordoghli *et al*. 2023). Lignin is known to degrade within a wide range of temperature due to its heterogeneous aromatic structure, that enhanced the formation of a stable carbonaceous char. Beyond 450 °C, the remaining weight is assigned to carbon and ash content.

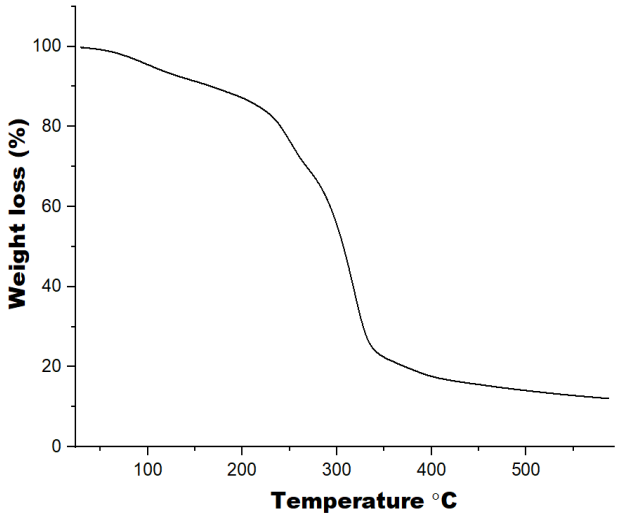


**Fig. 14.** TGA analysis of orange peel biochar

## FT-IR Investigation

The orange peel biochar's FT-IR spectra before and after $Pb^{2+}$ sorption, as shown in Fig. 15, reveal distinct changes in the surface functional groups, confirming the participation of oxygen-containing moieties in $Pb^{2+}$ uptake. The spectrum of OPB displays a small peak corresponding to –OH stretching at 3350 $cm^{-1}$, which is typical of hydroxyl and phenolic groups commonly reported in citrus-derived biochars (Zhang *et al*. 2022). After $Pb^{2+}$ uptake, this peak became more intense and shifted slightly to 3388 $cm^{-1}$, indicating ion exchange or coordination interactions between the surface hydroxyls and $Pb^{2+}$. The peaks seen at 1653 $cm^{-1}$ before and 1638 $cm^{-1}$ after Pb uptake are attributed to carbonyl/carboxylate and aromatic C=C groups, as well as shifts after metal sorption. This information is consistent with metal–carboxyl complexation reported for $Pb^{2+}$ sorption on lignocellulosic biochars (Mousa *et al*. 2025). The bands observed at 1162 $cm^{-1}$ before and 1077 to 1338 $cm^{-1}$ after are assigned to C–O stretching and the intensity stats to decrease after adsorption, suggesting their involvement in metal binding (Nandiyanto *et al*. 2025). The bands seen at 550 to 610 $cm^{-1}$ region are assigned to metal–oxygen (Pb–O) vibrations, affirming the formation of inner-sphere $Pb^{2+}$ complexes on the biochar surface.

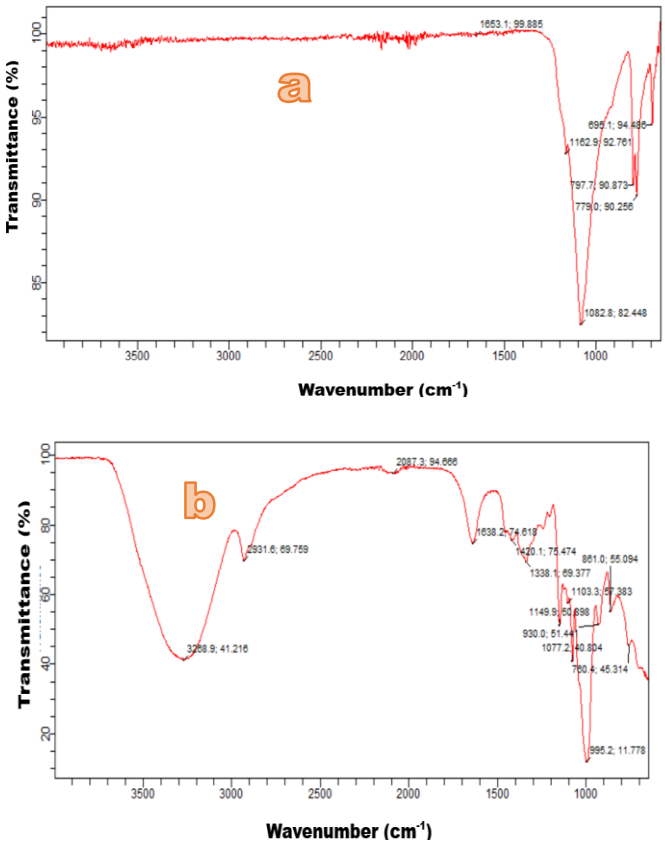


**Fig. 15.** The FT-IR analysis of orange peel biochar before (a) and after (b) $Pb^{2+}$ adsorption

## SEM Analysis

Prior to adsorption (Fig. 16a), the biochar surface displayed a rough, layered, and irregular morphology with fractured sheet-like structures.

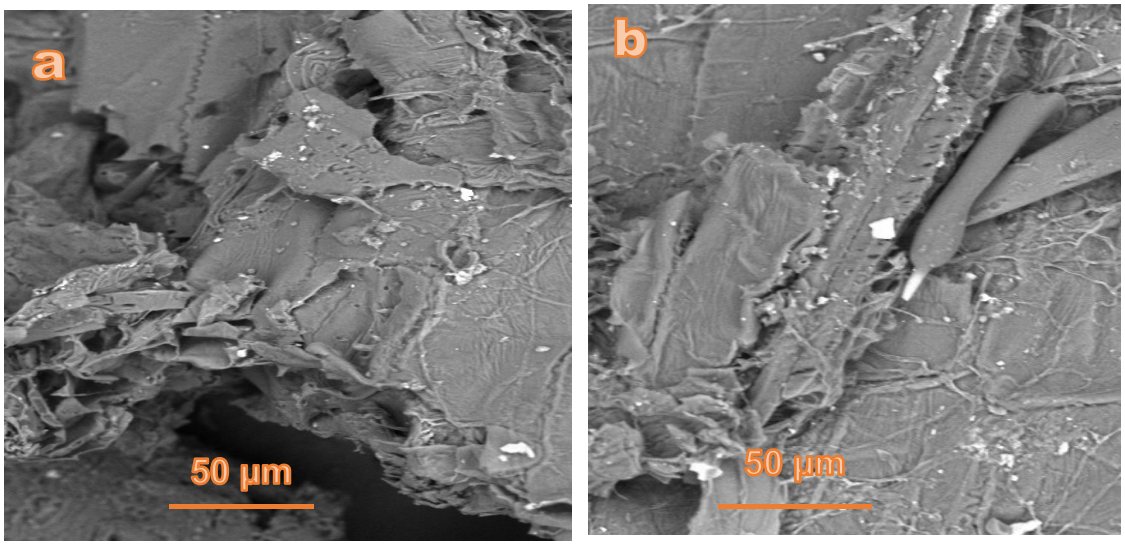


**Fig. 16.** The SEM images of OPB prior (a) and after $Pb^{2+}$ sorption (b)

This is typical of biochar derived from lignocellulosic biomass due to heterogeneous carbon formation during thermal degradation. The presence of visible pores suggests the availability of surface features that may facilitate pollutant interaction. Following $Pb^{2+}$ exposure (Fig. 16b), no substantial alteration in surface morphology is observed.

## Effect of Competing Ions

As displayed in Fig. 17, the presence of divalent alkaline earth metals significantly suppressed $Pb^{2+}$ uptake. The $Pb^{2+}$ removal decreased from 78% in single-solute systems to 52% and 55% in the presence of $Ca^{2+}$ and $Mg^{2+}$, respectively. This suppression can be attributed to direct competition for negatively charged surface functional groups such as –OH and $–COO^-$ and increased ionic strength, which lessens electrostatic attraction (Wu *et al.* 2021; Xu *et al.* 2022).

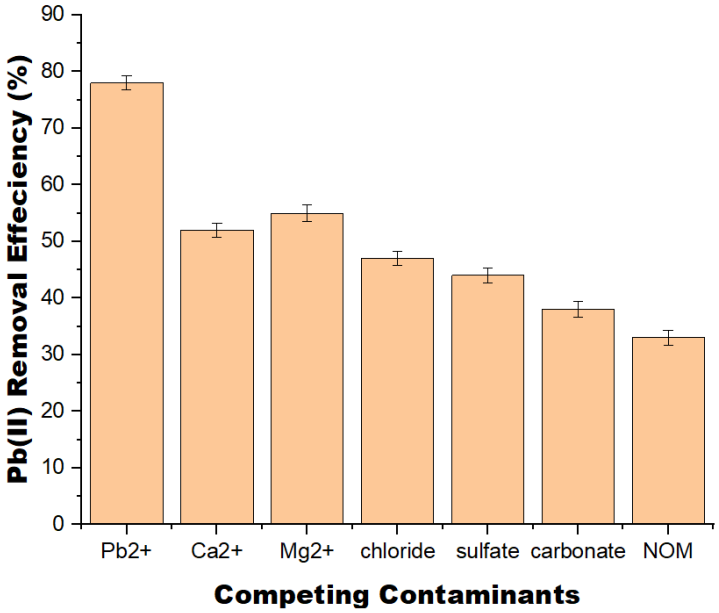


**Fig. 17.** Effect of competing cations, anions, and natural NOM on $Pb^{2+}$ uptake efficiency by orange peel biochar under optimized adsorption conditions

Anionic species also reduced $Pb^{2+}$ uptake behavior. Chloride and sulfate ions reduced $Pb^{2+}$ removal to 47% and 44%, respectively, due to aqueous Pb–Cl and Pb–$SO_4$ complex formation, which lowers the concentration of free $Pb^{2+}$ available for adsorption. Carbonate displayed a stronger inhibitory effect (38%), which may be because of the formation of stable Pb–carbonate species and surface site blocking (Chen *et al.* 2017; Shi *et al.* 2018). Surprisingly, the natural organic matter (NOM) induced the most pronounced reduction with $Pb^{2+}$ uptake reducing to 33%. This effect can be ascribed to complexation of $Pb^{2+}$ by humic substances in solution and pore/site blocking on the OPB surface, consistent with previous reports for biochar-based adsorbents (Song *et al.* 2025). These competition findings showed that although $Pb^{2+}$ removal by OPB is reduced in complex matrices, substantial removal efficiency is retained, indicating that OPB performance extends beyond ideal laboratory conditions and remains relevant for practical water treatment applications.

## CONCLUSIONS

This work evaluated the effectiveness and sustainability of biochar produced from orange peel (OPB) for the sorption of $Pb^{2+}$ from aqueous solution, and the following deductions were derived:

1. Orange peel biochar was found to have a porous, heterogeneous surface capable of adsorbing $Pb^{2+}$ from aqueous solution, with adsorption performance strongly impacted by solution pH, contact time, temperature, and initial metal concentration.
2. The Langmuir model indicated a maximum adsorption capacity of 73.5 mg/g, while the Freundlich model suggested a heterogeneous nature of the biochar surface.
3. The low mean adsorption energy obtained from the Dubinin–Radushkevich model, combined with thermodynamic data, shows that $Pb^{2+}$ sorption was governed mainly by physical adsorption mechanisms, including weak electrostatic interactions and pore-filling effects.
4. Thermodynamic analysis revealed that the process is endothermic and spontaneous, with enhanced haphazardness at the solid-solution interface.
5. The characterization results confirmed the presence of functional groups and a porous structure of the OPB which supports the adsorption process.
6. Overall, the orange peel biochar (OPB) presents a low-cost, renewable and efficient material for removing $Pb^{2+}$ from contaminated water, making it a promising option for sustainable remediation applications. Further investigations on fixed-bed column experiments, dynamic modeling, practical deployment and scale-up are needed for engineered water-treatment systems. In addition, testing at environmentally relevant low-concentration ranges (µg/L to low mg/L), along with validated QA/QC protocols, are important future work.

## ACKNOWLEDGMENTS

Princess Nourah bint Abdulrahman University Researchers Supporting Project number (PNURSP2026R76), Princess Nourah bint Abdulrahman University, Riyadh, Saudi Arabia. The authors extend their appreciation to the Deanship of Scientific Research at Northern Border University, Arar, KSA, for funding this research work through the project number "NBU-FFR-2026-2985-03"

### Authors Contributions

Ghaferah H. Al-Hazmi and Ali El-Rayyes: Contributed Resources, Software, Funding acquisition; Lamia A. Albedair: Project administration, Contributed Resources, Writing – Review & Editing; Edwin Andrew Ofudje: Conceptualization, Investigation, and supervised the work; Moamen S. Refat: Visualization, Validation, Writing – Review & Editing; Kholoud K. Alzahrani: Formal analysis, Software, Writing – Review & Editing; Oladejo Emmanuel Kola: Methodology, Data curation, Writing – Original Draft; All authors: Approval of final manuscript.

## REFERENCES CITED


Ademoyegun, A. J., Babarinde, N. A. A., and Ofudje, E. A. (2022). "Sorption of Pb (II), Cd (II), and Zn (II) ions from aqueous solution using *Thaumatococcus daniellii* leaves: Kinetic, isotherm, and thermodynamic studies," *Desalination and Water Treatment* 273, 162-171. https://doi.org/10.5004/dwt.2022.28877

Afolabi, F. O., and Musonge, P. (2023). "Synthesis, characterization, and biosorption of $Cu^{2+}$ and $Pb^{2+}$ ions from an aqueous solution using biochar derived from orange peels," *Molecules* 28(20), article 7050. https://doi.org/10.3390/molecules28207050

Afolabi, F. O., Musonge, P., and Bakare, B. F. (2021). "Bio-sorption of copper and lead ions in single and binary systems onto banana peels," *Cogent Engineering* 8(1), article 1886730. https://doi.org/10.1080/23311916.2021.1886730

Aigbe, R., and Kavaz, D. (2021). "Unravel the potential of zinc oxide nanoparticle-carbonized sawdust matrix for removal of lead (II) ions from aqueous solution," *Chinese J. Chem. Eng.* 29, 92-102. https://doi.org/10.1016/j.cjche.2020.05.007

Akhtar, N., Syakir Ishak, M. I., Bhawani, S. A., and Umar, K. (2021). "Various natural and anthropogenic factors responsible for water quality degradation: A review," *Water* 13(19), article 2660. https://doi.org/10.3390/w13192660

Arogundade, I., Hefnawy, M., Ofudje, E. A., El Gamal, A., and Emran, T. B. (2025). "$Pb^{2+}$ and $Cd^{2+}$ removal from aqueous solutions onto calcium-phosphate hydroxyl surface: Kinetics, isotherms and thermodynamic investigations," *Journal of Taibah University for Science* 19(1), article 2504745. https://doi.org/10.1080/16583655.2025.2504745

Azmi, L. S. (2025). "Membrane filtration technologies for sustainable industrial wastewater treatment: A review of heavy metal removal," *Desalination and Water Treatment* 2025, article 101321. https://doi.org/10.1016/j.dwt.2025.101321

Balali-Mood, M., Naseri, K., Tahergorabi, Z., Khazdair, M. R., and Sadeghi, M. (2021). "Toxic mechanisms of five heavy metals: Mercury, lead, chromium, cadmium, and arsenic," *Frontiers in Pharmacology* 12, article 643972. https://doi.org/10.3389/fphar.2021.643972

Benalia, A., Atime, L., Baatache, O., Khalfaoui, A., Ghomrani, A. F., Derbal, K., and Amirou, S. (2024). "Removal of lead in water by coagulation flocculation process using cactus-based natural coagulant: Optimization and modeling by response surface methodology (RSM)," *Environ. Monit. Assess.* 196(3), article 244. https://doi.org/10.1007/s10661-024-12412-9

Bouguettoucha, A., Chebli, D., Mekhalef, T., Nouia , A., and Amran, A. (2015). "The use of a forest waste biomass, cone of *Pinus brutia* for the removal of an anionic azo dye Congo red from aqueous medium," *Desalination and Water Treatment* 55(7), 1956-1965. https://10.1080/19443994.2014.928235

Briffa, J., Sinagra, E., and Blundell, R. (2020). "Heavy metal pollution in the environment and their toxicological effects on humans," *Heliyon* 6(9), article e04691. https://doi.org/10.1016/j.heliyon.2020.e04691

Chen, Y., Shi, J., Du, Q., Zhang, H., and Cui, Y. (2019). "Antibiotic removal by agricultural waste biochars with different forms of iron oxide," *RSC Adv.* 9(25), 14143-14153. https://doi.org/10.1039/c9ra01271k

Chen, D., Li, R., Bian, R., Li, L., Joseph, S., Crowley, D., and Pan, G. (2017). "Contribution of soluble minerals in biochar to $Pb^{2+}$ adsorption in aqueous solutions," *BioResources* 12(1), 1662-1679. https://10.15376/biores.12.1.1662-1679

Chowdhury, I. R., Chowdhury, S., Mazumder, M. A. J., and Al-Ahmed, A. (2022). "Removal of lead ions ($Pb^{2+}$) from water and wastewater: A review on the low-cost adsorbents," *Appl. Water Sci.* 12(8), article 185. https://doi.org/10.1007/s13201-022-01703-6

Din, S. U., Al-Ahmary, K. M., AlMohamadi, H., Al-Mhyawi, S. R., Alrashood, J. S., Ngueagni, P. T., and Ofudje, E. A. (2025). "Low-cost and sustainable bioadsorbent from banana peel waste for crystal violet dye removal," *BioResources* 20(4), 10640-10664. https://doi.org/10.15376/biores.20.4.10640-10664

Dubinin, M. M. (1960). "The potential theory of adsorption of gases and vapors for adsorbents with energetically nonuniform surfaces," *Chemical Reviews* 60, 235-241. https://doi.org/10.1021/cr60204a006

El Hammari, L., Latifi, S., Saoiabi, S., Azzaoui, A. K., Hammouti, B., Chetouani, A., and Sabbahi, R. (2022). "Toxic heavy metals removal from river water using a porous phospho-calcic hydroxyapatite," *Moroccan Journal of Chemistry* 10(1), article 31752. https://doi.org/10.48317/IMIST.PRSM/morjchem-v10i1.31752

El-Rayyes, A., Arogundade, I., Ofudje, E. A., Refat, M. S., Alsuhaibani, A. M., Akande, J. A., and Sodiya, E. F. (2025). "Thermodynamic, isotherm and kinetic studies lead ions adsorption onto *Manihot esculenta* chaff surface," *Sci. Rep.* 15(1), article 27672. https://doi.org/10.1038/s41598-025-09307-1

Gargiulo, V., Di Natale, F., and Alfe, M. (2024). "From agricultural wastes to advanced materials for environmental applications: Rice husk-derived adsorbents for heavy metals removal from wastewater," *J. Environ. Chem. Eng.* 12(5), article 113497. https://doi.org/10.1016/j.jece.2024.113497

Ghori, N. H., Ghori, T., Hayat, M. Q., Imadi, S. R., Gul, A., Altay, V., and Ozturk, M. (2019). "Heavy metal stress and responses in plants," *Int. J. Environ. Sci. Technol.* 16(3), 1807-1828. https://doi.org/10.1007/s13762-019-02215-8

Ghosh, N., Sen S., Biswas G., Saxena A., and Haldar P.K. (2023). "Adsorption and desorption study of reusable magnetic iron oxide nanoparticles modified with *Justicia adhatoda* leaf extract for the removal of textile dye and antibiotic," *Water Air Soil Pollut*. 234(3), article 202. https://doi.org/10.1007/s11270-023-06217-8

Hubbe, M. A., Azizian, S., and Douven, S. (2019). "Implications of apparent pseudo-second-order adsorption kinetics onto cellulosic materials. A review," *BioResources* 14(3), 7582-7626. https://doi.org/10.15376/biores.14.3.7582-7626

Jasim, A. Q., and Ajjam, S. K. (2024). "Removal of heavy metal ions from wastewater using ion exchange resin in a batch process with kinetic isotherm," *South Afr. J. Chem. Eng.* 49(1), 43-54. https://doi.org/10.1016/j.sajce.2024.04.002

Jjagwe, J., Olupot, P. W., Menya, E., and Kalibbala, H. M. (2021). "Synthesis and application of granular activated carbon from biomass waste materials for water treatment: A review," *J. Bioresour. Bioprod.* 6(4), 292-322. https://doi.org/10.1016/j.jobab.2021.03.003

John B. D., King, P., and Prasanna Kumar, Y. (2019). "Optimization of Cu (II) biosorption onto sea urchin test using response surface methodology and artificial neural networks," *Int. J. Environ. Sci. and Technol.* 16(4), 1885-1896. https://doi.org/10.1007/s13762-018-1747-2

Khan, A., Khan, S. K. M. A., Khan, M. A., Aamir, M., Ullah, H., Nawab, J., and Shah, J. (2019). "Heavy metals effects on plant growth and dietary intake of trace metals in vegetables cultivated in contaminated soil," *Int. J. Environ. Sci. and Technol.* 16(5), 2295-2304. https://doi.org/10.1007/s13762-018-1849-x

Kordoghli, S., Fassatoui, E., Largeau, J. F., and Khiari, B. (2023). "Slow pyrolysis of orange peels blended with agro-food wastes: Characterization of the biochars for environmental applications," *Comptes Rendus. Chimie, Materials and Clean Processes for Sustainable Energy and Environmental Applications* 26, 37-51. https://doi.org/10.5802/crchim.240

Kori, A. K., Ramavandi, B., Mahmoodi, S. M. M., and Javanmardi, F. (2024). "Magnetization and ZIF-67 modification of *Aspergillus flavus* biomass for tetracycline removal from aqueous solutions: A stable and efficient composite," *Environ. Res.* 252(Pt 2), article 118931. https://doi.org/10.1016/j.envres.2024.118931

Lupa, L., Maranescu, B., and Visa, A. (2018). "Equilibrium and kinetic studies of chromium ions adsorption on Co (II)-based phosphonate metal organic frameworks," *Sep. Sci. Technol.* 53(7), 1017-1026. https://doi.org/10.1080/01496395.2017.1340953

Mahdi, Z., Yu, Q. J., and El Hanandeh, A. (2018). "Removal of lead (II) from aqueous solution using date seed-derived biochar: Batch and column studies," *Appl. Water Sci.* 8(6), article 181. https://doi.org/10.1007/s13201-018-0829-0

Mandal, S., Calderon, J., Marpu, S. B., Omary, M. A., and Shi, S. Q. (2021). "Mesoporous activated carbon as a green adsorbent for the removal of heavy metals and Congo Red: Characterization, adsorption kinetics, and isotherm studies," *Journal of Contaminant Hydrology* 243, article 103869. https://doi.org/10.1016/j.jconhyd.2021.103869

Meng, K., Dong, Y., Liu, J., Xie, J., Jin, Q., Lu, Y., and Lin, H. (2025). "Advances in selective heavy metal removal from water using biochar: A comprehensive review of mechanisms and modifications," *J. Environ. Chem. Eng.* 2025, article 116099. https://doi.org/10/1016/j.jece.2025.116099

Michael-Igolima, U., Abbey, S. J., Ifelebuegu, A. O., and Eyo, E. U. (2023). "Modified orange peel waste as a sustainable material for adsorption of contaminants," *Materials* 16(3), article 1092. https://doi.org/10.3390/ma16031092

Minh, V. C., Lien, N. T. L., Thuy, N. T., Phung, L. T. K., and Huy, N. N. (2023). "Production of biochar from coconut husks for adsorption of heavy metals in water," *Philippine Journal of Science* 152(5), 1579-1593. https://doi.org/10.56899/152.05.05

Mishra, S., Bharagava, R. N., More, N., Yadav, A., Zainith, S., Mani, S., and Chowdhary, P. (2019). "Heavy metal contamination: An alarming threat to environment and human health," in: *Environmental Biotechnology: For Sustainable Future*, pp. 103-125. https://doi.org/10.1007/978-981-10-7284-0_5

Mohrazi, A., and Ghasemi-Fasaei, R. (2023). "Removal of methylene blue dye from aqueous solution using an efficient chitosan-pectin bio-adsorbent: Kinetics and isotherm studies," *Environ. Monit. Assess*. 195(2), article 339. https://doi.org/10.1007/s10661-022-10900-4

Mohubedu, R. P., Diagboya, P. N., Abasi, C. Y., Dikio, E. D., and Mtunzi, F. (2019). "Magnetic valorization of biomass and biochar of a typical plant nuisance for toxic metals contaminated water treatment," *J. Clean. Prod.* 209, 1016-1024. https://doi.org/10.1016/j.jclepro.2018.10.215

Mousa, S., Dubdub, I., Alfaiad, M. A., Younes, M. Y., and Ismail, M. A. (2025). "Characterization and kinetic study of agricultural biomass orange peel waste combustion using TGA data," *Polymers (Basel)* 17(8), article 1113. https://doi.org/10.3390/polym17081113

Mustapha, S. I., Aderibigbe, F. A., Adewoye, T. L., Mohammed, I. A., and Odey, T. O. (2021). "Silver and titanium oxides for the removal of phenols from pharmaceutical

wastewater," *Mater Today: Proc.* 38, 816-822. https://doi.org/10.1016/j.matpr.2020.04.669

Nandiyanto, A. B., Nugraha, A. Y., Fawwaz, L. T., Pramajati, M. F., Wijaya, Y. T., Fiandini, M., Bilad, M. R., Kurniawan, T., Gandidi, I. M., and Sukrawan, Y. (2025). "Utilization of orange peel-derived biochar for ammonia adsorption: Isotherm analysis and hydrogen storage prospective for supporting sustainable development goals (SDGS)," *J. Eng. Sci. Technol.* 20(1), 85-98.

Negroiu, M., Țurcanu, A. A., Matei, E., Râpă, M., Covaliu, C. I., Predescu, A. M., and Predescu, C. (2021). "Novel adsorbent based on banana peel waste for removal of heavy metal ions from synthetic solutions," *Materials* 14(14), article 3946. https://doi.org/10.3390/ma14143946

Ngueagni, P. T., Hefnawy, M., Ofudje, E. A., El Gamal, A., Akande, J. A., and Emran, T. B. (2025). "Cellulose-based adsorbent of animal waste for the adsorption of lead and phenol," *BioResources* 20(2), 3923-3952. https://doi.org.10.15376/biores.20.2.3923-3952

Niu, Z., Feng, W., Huang, H., Wang, B., Chen, L., Miao, Y., and Su, S. (2020). "Green synthesis of a novel Mn–Zn ferrite/biochar composite from waste batteries and pine sawdust for $Pb^{2+}$ removal," *Chemosphere* 252, article 126529. https://doi.org/10.1016/j.chemosphere.2020.126529

Ofudje, E. A., Al-Ahmary, K. M., Alzahrani, E. A., Ud Din, S., and Al-Otaibi, J. S. (2024). "Sugarcane peel ash as a sorbent for methylene blue," *BioResources* 19(4), 9191-9219. https://doi.org/10.15376/biores.19.4.9191-9219

Ofudje, E. A., Sodiya, E. F., Olanrele, O. S., and Akinwunmi, F. (2023). "Adsorption of $Cd^{2+}$ onto apatite surface: Equilibrium, kinetics and thermodynamic studies," *Heliyon* 9(2), article e12971. https://doi.org/10.1016/j.heliyon.2023.e12971

Ogundiran, A. A., Ofudje, E. A., Ogundiran, O. O., and Adewusi, A. M. (2022). "Cationic dye adsorptions by eggshell waste: Kinetics, isotherms and thermodynamics studies," *Desalination & Water Treatment* 280, 157-167. https://doi.org/10.5004/dwt.2022.29080

Onyekwere, O. S., Hambali, H. U., Macaulay, F. E., Haruna, A. D., Ayinla, L., Ogundokun, P. B., and Hayes, A. I. (2024). "Modified corn cob adsorbent for heavy metal removal from wastewater," *Savannah J. Sci. Eng. Technol.* 2(02), 33-40. https://doi.org/10.1016/sajset-02-2024-0010

Rahman, A., Yoshida, K., Islam, M. M., and Kobayashi, G. (2023). "Investigation of efficient adsorption of toxic heavy metals (chromium, lead, cadmium) from aquatic environment using orange peel cellulose as adsorbent," *Sustainability* 15(5), article 4470. https://doi.org/10.3390/su15054470

Raman, N. M., Asokan, S., Shobana Sundari, N., and Ramasamy, S. (2018). "Bioremediation of chromium (VI) by *Stenotrophomonas maltophilia* isolated from tannery effluent," *Int. J. Environ. Sci. Technol.* 15(1), 207-216. https://doi.org/10.1007/s13762-017-1378-z

Shi, Q., Sterbinsky, G.E., Prigiobbe, V., and Meng, X. (2018). "Mechanistic study of lead adsorption on activated carbon," *Langmuir* 34(45), 13565-13573. https://doi.org/10.1021/acs.langmuir.8b03096

Singh, V., Pant, N., Sharma, R. K., Padalia, D., Rawat, P. S., Goswami, R., Singh, P., Kumar, A., Bhandari, P., Tabish, A., and Deifalla, A. M. (2023). "Adsorption studies of Pb (II) and Cd (II) heavy metal ions from aqueous solutions using a magnetic

biochar composite material," *Separations* 10(7), article 389. https://doi.org/10.3390/separations10070389

Sireesha, C., Durairaj, K., Balasubramanian, B., Sumithra, S., Subha, R., Kamyab, H., and Chelliapan, S. (2025). "Process development of guava leaves with alkali in removal of zinc ions from synthetic wastewater," *Journal of the Taiwan Institute of Chemical Engineers* 166, article 105283. https://doi.org/10.1016/j.jtice.2023.105283

Song, C., Liu, J., Zhang, L., Wang, J., and Shu, X. (2025). "Competitive adsorption of $Pb^{2+}$ from aqueous solutions by multi-source lignocellulose-derived hydrothermal humic acid," *Processes* 13(1), article 155. https://doi.org/10.3390/pr13010155

Wu, Q., Dong, S., Wang, L., and Li, X. (2021). "Single and competitive adsorption behaviors of $Cu^{2+}$, $Pb^{2+}$ and $Zn^{2+}$ on the biochar and magnetic biochar of pomelo peel in aqueous solution," *Water* 13(6), article 868. https://doi.org/10.3390/w13060868

Vidal, R. R. L., and Moraes, J. S. (2019). "Removal of organic pollutants from wastewater using chitosan: A literature review," *Int. J. Environ. Sci. Technol.* 16(3), 1741-1754. https://doi.org/10.1007/s13762-018-2061-8

Wang, Q., Wang, Y., Yuan, L., Zou, T., Zhang, W., Zhang, X., Zhang, L., and Huang, X. (2022). "Utilization of low-cost watermelon rind for efficient removal of Cd (II) from aqueous solutions: Adsorption performance and mechanism elucidation," *Chem. Eng. J. Adv.* 12, article 100393. https://doi.org/10.1016/j.ceja.2022.100393

Xu, Y., Qu, Y., Yang, Y., Qu, B., Shan, R., Yuan, H., and Sun, Y. (2022). "Study on efficient adsorption mechanism of $Pb^{2+}$ by magnetic coconut biochar," *International Journal of Molecular Sciences 23*(22), article 14053. https://doi.org/10.3390/ijms232214053

Zhang, W., Wang, Y., Fan, L., Liu, X., Cao, W., Ai, H., Wang, Z., Liu, X., and Jia, H. (2022). "Sorbent properties of orange peel-based biochar for different pollutants in water," *Processes* 10(5), article 856. https://doi.org/10.3390/pr10050856

Zhao, T., Yao, Y., Li, D., Wu, F., Zhang, C., and Gao, B. (2018). "Facile low-temperature one-step synthesis of pomelo peel biochar under air atmosphere and its adsorption behaviors for Ag (I) and Pb (II)," *Science of The Total Environment* 640, 73-79. https://doi.org/10.1016/j.scitotenv.2018.05.251

Zheng, E., Feng, G., Jiang, F., Shao, C., Fu, H., Hu, Z., and Liu, J. (2024). "Effect of process parameters on the synthesis and lead ions removal performance of novel porous hydroxyapatite sheets prepared *via* non-aqueous precipitation method," *Ceramics International* 50(7), 10897-10905. https://doi.org/10.1016/j.ceramint.2023.12.406

Article submitted: November 26, 2025; Peer review completed: January 18, 2026; Revised version received: January 28, 2026; Further revised version accepted: February 16, 2026; Published: March 9, 2026.
DOI: 10.15376/biores.21.2.3831-3855